A Method for Material Parameter Determination for the Human Mandible Based on Simulation and Experiment *

Christian Clason
Center for Mathematical Sciences, Munich University of Technology
85747 Garching bei München, Germany
clason@ma.tum.de

Andreas M. Hinz
Center for Mathematical Sciences, Munich University of Technology
85747 Garching bei München, Germany
hinz@ma.tum.de

Heinrich Schieferstein
Department for Orthopedics, Section Biomechanics, Munich University of Technology
Connollystraße 32, 80809 München, Germany
schieferstein@alumni.tum.de

Abstract

In cranio-maxillofacial surgery planning and implant design, it is important to know the elastic response of the mandible to load forces as they occur, e.g., in biting. The goal of the present study is to provide a method for a quantitative determination of material parameters for the human jaw bone, whose values can, e.g., be used to devise a prototype plastic model for the mandible. Non-destructive load experiments are performed on a cadaveric mandible using a specially designed test bed. The identical physiological situation is simulated in a computer program. The underlying mathematical model is based on a two component, linear elastic material law. The numerical realization of the model, difficult due to the complex geometry and morphology of the mandible, is via the finite element method. Combining the validated simulation with the results of the tests, an inverse problem for the determination of Young's modulus and the Poisson ratio of both cortical and cancellous bone can then be solved.

Keywords: mandible, finite element method, validation, material properties, inverse problem.

1 Introduction

At the onset, the goal of this combined in vitro and in silico study on the elastic response of the human lower jaw bone (the mandible) to mechanical loads was the design of a reliable tool for the cranio-maxillofacial surgeon to plan operations using different techniques. The medical indications are either inborn severe defects of the mandible or those coming from accidents or diseases. The methods of surgical treatment are plentiful, depending on the kind of defect, but also on the individual situation of the patient. Let us just mention osteosynthesis, where plates are applied to the bone to support the development of new bone material in fractures (cf. [21]), and distraction, where a mechanical device, the distractor, is bridging a gap between two parts of

the bone allowing these two parts to be separated from each other and afterwards joined by newly developed bone material. A current approach to surgical planning is to produce plastic models of the patient's mandible, the geometry of which having been registered by computerized tomography (CT), using techniques like rapid prototyping (cf. [29]). The models, together with the implants, are then subjected to a couple of load cases in biomechanical tests to optimize arrangement and specifications of the implants. Yet their stability in vivo will depend significantly on the elastic properties of the patient's mandible. Therefore, it is desirable for these to be taken into account in the lay-out of the model as well.

However, the material properties of bone vary considerably from one individual to another and are impossible to determine in vivo. It is known that bone is an inhomogeneous, anisotropic material, and the literature reports a wide range of values for material parameters [11, 20, 24]. Experimental measurement techniques are complicated by the anisotropy and the complex geometry of the mandible. They are either destructive or employ non-physiological test loads (cf. [28]). In vivo experiments with animals are not viable due to the different morphology. The possibility to use cadaveric human bones is restricted by availability and the fact that once dead, bone changes its elastic properties rapidly. A realistic goal is therefore to improve rapid prototyping models by providing a standardized value for the elasticity modulus which closely represents the elastic behavior of an average human mandible (cf. [6] for the case of the tibia) in typical physiological load situations.

Since testing and numerical methods are closely interwoven today, a promising approach seemed to be to combine experiments with computer simulations. There are a number of challenging tasks involved in devising the underlying mathematical model and its realization as a computer simulation. First of all, the geometry of the mandible is much more complex and variable than that of other human bones like the tibia. Moreover, the muscle forces are essentially unknown, since existing models (cf. [23, 16]) have not yet been validated.

In view of the irregularity of the domain and the complexity of the boundary conditions, the finite element (FE) approach is the most suitable numerical method in our case. It has been employed successfully for more regular bones like the femur and tibia. For the mandible, however, the first fully three-dimensional simulation is described in [17]. Their model takes into account all types of tissue involved, namely bone, skin, teeth and dental enamel. In particular, the bone tissue was modeled as orthotropic. However, the grid with around 5,500 nodes is too coarse to represent the geometry of individual mandibles adequately.

In [10], the bone was modeled as (locally) transverse isotropic. A grid of 20-noded hexahedral elements with around 10,000 nodes was employed. This was accompanied by a convergence analysis proving this number of nodes to be appropriate. On the other hand, material properties were taken from published data for the tibia.

Both models reflect simple load cases quite satisfactorily. However, due to the layer-based grid generation, important details of the geometry were ignored. Moreover, they took over material data from the literature, whose reliability could be questioned. Later approaches (cf. [8]) use more sophisticated geometries, but also rely on previous literature for material properties and validation.

In this paper, we present a new method to determine material parameters, based on a parallel experimental and simulation set-up specifically designed for this purpose, validated on a single cadaveric human mandible. We will first describe the experiment on the biomechanical test bed *Mandibulator*, which can be used to impose any reasonable load configuration on either plastic models of the mandible or on cadaveric human mandibles. It is supported by a video system to capture the elastic response of the specimen. We then present the mathematical model for the elastic behavior of the mandible which is the basis for the numerical simulation. The results of this simulation are then compared with the measurements from the experiment for validation. This combination of experiment and simulation allows for a mathematical parameter identification to determine material parameters for the bone. The justification for this kind of material parameter determination stems from the fact that it is non-destructive and more viable, because mandibular bone material, which is inhomogeneous and geometrically rather complex, is not readily available

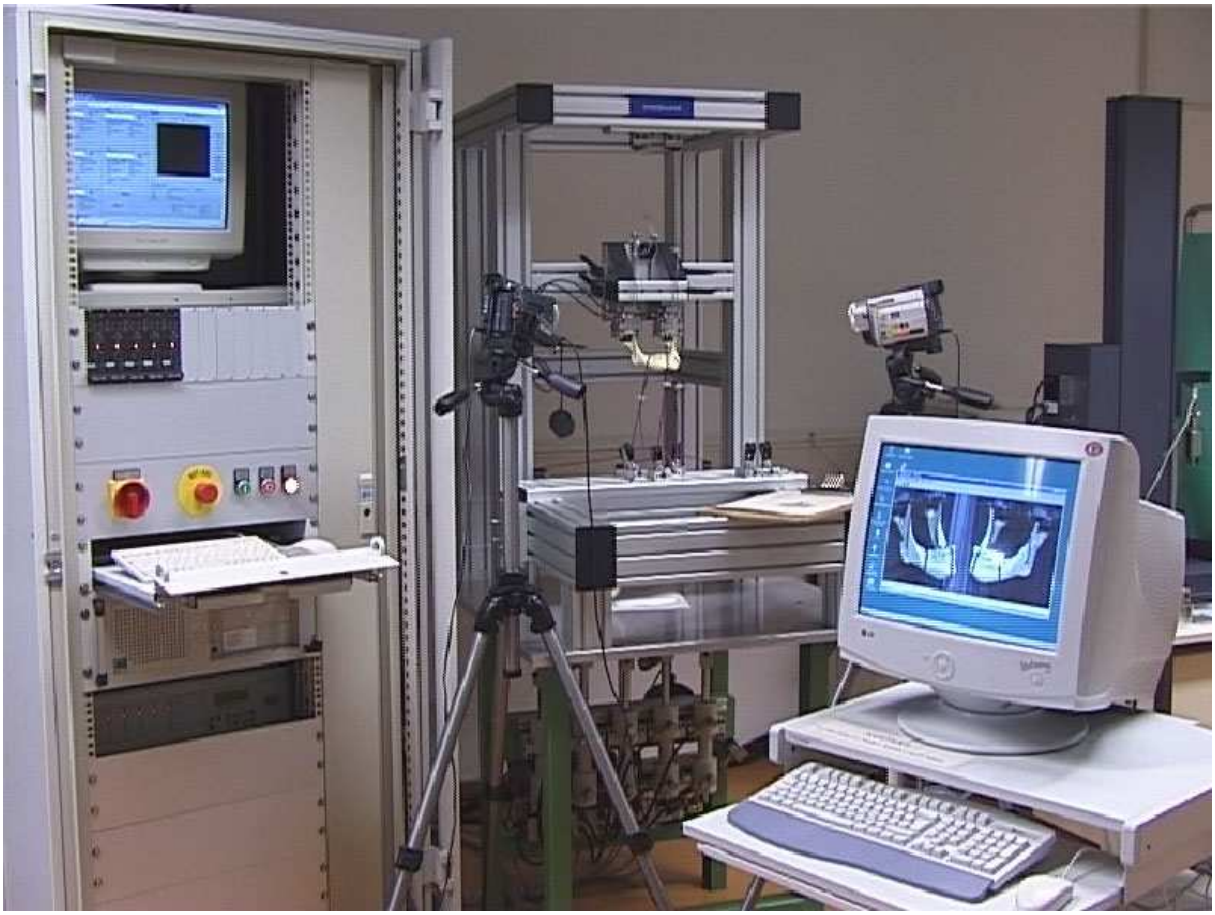

Figure 1: General view of the Mandibulator.

for standard mechanical measurements. Since both the experiment and the simulation start off from the *same* geometrical object, which is subjected to *identical* constraints and load configurations, this is the first time that a direct comparison of in vitro and in silico experiments on the human mandible has been performed.

2 Materials and methods

2.1 Experimental set-up

The set-up employed in our investigation has been developed specifically for static and dynamic experiments with the human mandible or an artificial model of it. This Mandibulator consists of three essential components (see Figure 1, cf. [25]):

- a modular rig holding specimen, sensors, cameras and actuators,
- a PC for data processing and steering the control units for the hydraulic drives,
- a motion capture system consisting of up to three cameras and a computer.

Hydraulic drives were chosen for load application. These can create forces ranging from 0 to 1,000N. Alternatively, eleven of the sixteen drives can be controlled in the range of 0 to 100mm.

The force diversion is realized by stretch-free Nylon ropes and blocks with ball bearings which can be considered frictionless. Therefore, the force at the point where the rope is attached to the mandible is the same as the force applied by the cylinder. Each hydraulic cylinder is equipped with a force sensor.

The PC is used for both experiment control and data acquisition. Programming is realized under LabVIEW^{TM} 6i allowing for an individual addressing of the drives with a simultaneous recording of force/displacement values and reacting forces. A digital-analog converter provides the analog output signal for the hydraulic control units as well as the acquisition of 42 parameters. All data are saved to disk for off-line analysis. At the sampling rate of 1kHz, each force signal has a resolution of 12bit (for 1,000N or 100mm).

Due to the clinical background mentioned above, a system for tension measurement would not give the required information (i.e. the relative motion of mandibular fragments under load). Therefore, we were primarily interested in the resulting displacements. These deformations are recorded by the digital cameras observing the positions of tracking markers. From this, a motion capture system (SIMI°Motion^{TM} 6) computes the spatial marker displacements. These data can be visualized or stored for further analysis.

2.2 Mathematical model and numerical simulation

The main problems in modeling the human mandible arise from the extremely irregular shape of this bone and its complex morphology. These features vary substantially inter-individually and are in addition subject to time-dependent adaptations. Moreover, bearing and application of forces are not yet well understood. As our approach is in aim of improving prototype mandibles, we decided to focus on accuracy in the geometrical representation, while trying to determine representative material parameters corresponding to load cases of interest in applications. We therefore chose an experimental and a simulation set-up which is rather elementary but has physiologically realistic features. As an example for a clinically relevant situation, we defined a load as produced by a static incisal bite, modeled as a central downward force perpendicular to the alveolar ridge. For the masticular muscles we made the reduction to the pterygo-masseter sling, which loops around the jaw angle and pulls upward. As we were only considering static load cases with the condyles fixed (cf. infra), we neglected all muscle groups related to the temporomandibular joint (TMJ).

A direct measurement of muscle forces is not possible in vivo. They are estimated, e.g., by measuring the activation of the muscle by electromyography and relating the stimulation heuristically to the cross-sectional area of the muscle. The values of muscle forces vary considerably in literature (cf. [19, 14]). The load forces we chose to apply ranged up to 650N. This covers the physiologically reasonable range from 65N (cf. [12]) to 500N (cf. [9]).

A further boundary condition occurs at the TMJ. This is a very complicated issue (cf. [2]) due to a variety of possible movements with different groups of muscles involved. It leads to a contact boundary condition with friction whose mathematical models are not yet sufficiently studied. We therefore limited ourselves deliberately to homogeneous Dirichlet boundary conditions at the condyles, i.e. they are fixed in space. By this bias, there is no rigid body movement, thus guaranteeing uniqueness of the mathematical solution. Special care was taken in the experiment to realize a tension-free mounting of the specimen. We are, of course, well aware of the crudeness of this neglect. See [15, 18] for recent approaches to this problem.

For the elastic response, we chose a linear material law, supported by the fact that the displacements which occur in our study are small. Since inhomogeneities vary considerably between individuals, and since one of our goals was to describe a "standard" smoothing these differences out, we are assuming two homogeneous isotropic components (cortical and cancellous bone, respectively). Our choice of an isotropic as opposed to orthotropic or transversally isotropic material was motivated by the fact that the symmetry axes can not be recovered directly from the CT data available and that we wanted to avoid another mathematical identification problem. Moreover, manufacturing a standard model from isotropic material is much more feasible. The elastic

properties in the isotropic material are given by *Young's modulus* E (in Pa) and the *Poisson ratio* ν.

The displacements as resulting from the load can then be represented mathematically as the solution of a second order elliptic boundary value problem.

Problem 2.1. *Let* $\Omega \subset \mathbb{R}^3$, $\Gamma_0 \subset \partial\Omega$, $\Gamma_1 \subset \partial\Omega$, $\Omega_1 \subset \Omega$ *and* $\Omega_2 = \Omega \setminus \overline{\Omega}_1$. *Further we are given the function* $g : \Gamma_1 \to \mathbb{R}^3$ *and the* Lamé constants λ_i *and* μ_i *on* Ω_i, *respectively.*

We look for a function $u : \overline{\Omega} \to \mathbb{R}^3$ *with*

$$-\mathbf{div}(\boldsymbol{\sigma}(\boldsymbol{\varepsilon}(u)))(x) = 0, \qquad x \in \Omega\,, \tag{1}$$

$$u(x) = 0, \qquad x \in \Gamma_0\,, \tag{2}$$

$$(\boldsymbol{\sigma}(\boldsymbol{\varepsilon}(u)))(x)\mathbf{n}(x) = g(x), \quad x \in \Gamma_1\,, \tag{3}$$

where

$$\boldsymbol{\sigma}(\boldsymbol{\varepsilon}) = \lambda_1(\mathbf{trace}\,\boldsymbol{\varepsilon})\mathbf{I} + 2\mu_1\boldsymbol{\varepsilon} \text{ on } \Omega_1, \tag{4}$$

$$\boldsymbol{\sigma}(\boldsymbol{\varepsilon}) = \lambda_2(\mathbf{trace}\,\boldsymbol{\varepsilon})\mathbf{I} + 2\mu_2\boldsymbol{\varepsilon} \text{ on } \Omega_2, \tag{5}$$

$$\boldsymbol{\varepsilon}(u) = \frac{1}{2}(\nabla u^T + \nabla u). \tag{6}$$

In this context, Ω_1 and Ω_2 stand for regions of cortical and cancellous bone, respectively, and $u(x)$ denotes the displacements of each point $x \in \Omega$, if the body Ω is subjected to forces (represented by g) acting on part of its surface. The Lamé constants are related to Young's modulus and the Poisson ratio by the formulas $\mu = \frac{E}{2\,(1+\nu)}$, $\lambda = \frac{\nu E}{(1+\nu)(1-2\nu)}$.

The FE method is the appropriate setting for the numerical solution of Problem 2.1. It is frequently used in structural mechanics and has established itself as a standard tool in the biomechanical analysis of bones. For the general mathematical background we refer to [4] and [5, §§2.4, 2.6 and 4]; for the application to elasticity, cf. [3].

Since we were dealing with isotropic materials, we used linear tetrahedral finite elements in order to achieve acceptable performance for the simulation to be used in our inverse problem. Additionally, tetrahedral elements guarantee an admissible triangulation for any geometry, as opposed to hexahedral elements. Important for the convergence of the procedure is the quality of the triangulation used. A measure for this is either an upper bound for the ratio of the radii of the circumscribed and inscribed spheres or a bound for the obtuseness of the inner angles (cf. [13]). For $u \in H^2(\Omega)^3$, the theorem of Aubin and Nitsche then guarantees quadratic convergence from the estimate

$$\|u - u_h\|_0 \le Ch^2\,|u|_2\,. \tag{7}$$

2.3 Experiment and simulation

As a specimen, we used an alcohol preserved cadaveric mandible. Because we wanted to keep the mathematical model as simple as possible, we avoided complicated contact boundary conditions at the condyles where the mandible attaches to the TMJ, thus considering the mandible as an independent entity. For better comparison, we therefore chose in our experiments to fix the mandible in the rig by plastering the condyles in artificial joint pits, thus avoiding rigid body movements. The masseter muscles and bite forces were simulated by ropes.

The masseter muscles were included in order to prevent high collum fractures or a force concentration in the higher collum area, which is the weakest part of the mandible when the joints are subjected to a load situation. Six marker points were attached to the body of the mandible at carefully chosen locations (see Figure 2). Two cameras were set up with different angles of view on the specimen. We first calibrated the geometrical situation with a pair of pictures including an exactly specified reference grid, then took a set of pictures of the load free mandible. Taking into

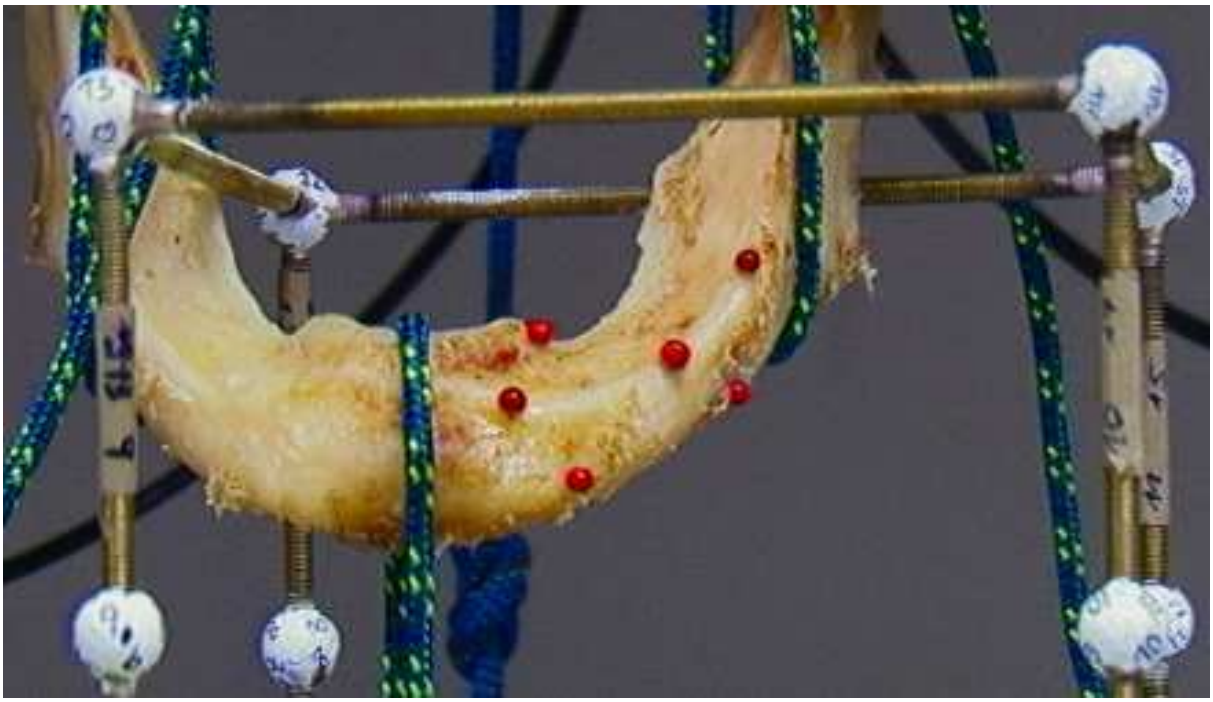

Figure 2: Frontal view of specimen with rope slings and marker points attached.

consideration the leverage in the lateral view, an incisal bite force was chosen twice or three times the value of the muscle forces. This situation should prevent a collum fracture. The position of the mandible and the direction of the forces applied correspond to a nearly shut mouth biting a pen. (Other situations like crunching food are more complex because of the asymmetrical joint loads and dental load distribution, not to mention the unknown muscular activity.) The same load experiment, with forces ranging up to 650N in steps of 50N, was repeated after the specimen had been soaked in Ringer's solution for 16 hours.

The set of pictures was imported into SIMI°Motion$^{\mathrm{TM}}$. After the markers were tracked in both views for each configuration with an accuracy of $5 \cdot 10^{-5}$m, SIMI°Motion$^{\mathrm{TM}}$ calculated the three-dimensional displacements of the six marker points.

After the experiments were finished, the specimen was removed from the test bed with the fixations still attached to it. A CT scan was performed of this whole object, and the resulting stack of slices imported into the software amira$^{\mathrm{TM}}$ (Zuse Institute Berlin) which specializes in medical data visualization. There, the voxel data were segmented into volume sets representing the mandible, condylar fixations and the ropes. Cortical and cancellous bone was distinguished by semi-automatic thresholding (a grey value of 600HU marked the border, with manual postprocessing to correct obvious errors), and assigned to different regions. By a modified marching cube method, the boundary between the different regions (and the exterior) was converted into triangular surfaces. This provided us with two volumes (cortical and cancellous bone, respectively), the interface between them, as well as exact representations of the areas where the mandible was held fixed or subjected to forces.

The resulting data set was too large to be dealt with numerically in adequate time. Therefore, an edge reduction algorithm was employed to reduce the number of surface triangles to 15,000, which captures the features of the original geometry sufficiently, as well as being manageable. After checking the triangular grid for holes, degenerate triangles and flipped orientations (which would pose severe numerical problems for the FE simulation), the method of advancing fronts was used to fill the bone regions with a tetrahedral grid. This final volume grid consisted of 10,409

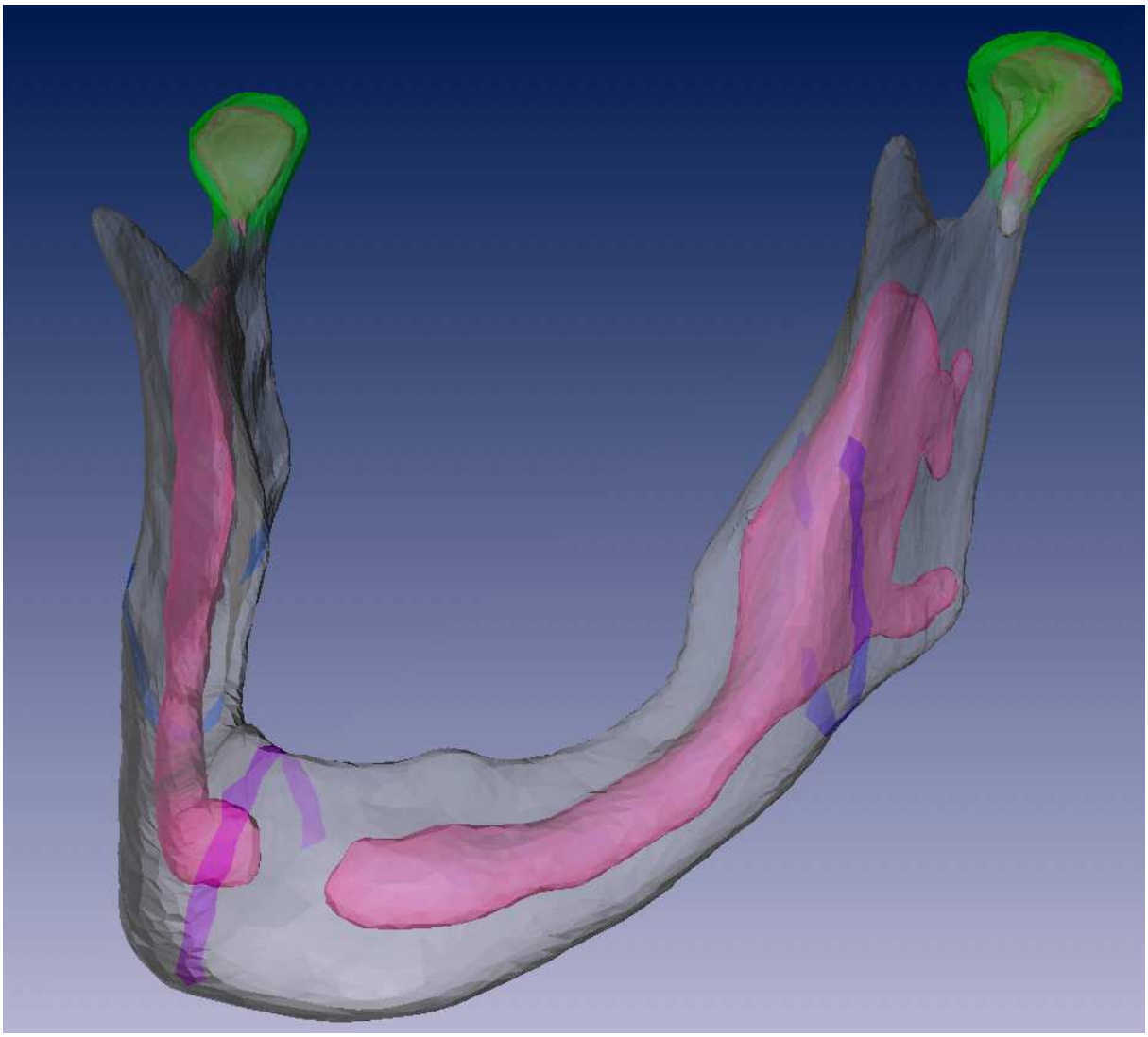

Figure 3: Generated volume grid segmented into cortical and cancellous bone, and with boundary conditions designated.

nodes, 45,913 tetrahedra (11,117 of which were considered cancellous bone) and 96,966 triangles (see Figure 3). Further tests displayed the stability of the results with respect to increasing fineness of the grid.

Using the developer edition of amira$^{\mathrm{TM}}$, we were able to extend this software with output modules to transfer the generated grid to the FE software. Similarly, input modules allowed the results of our simulation to be visualized using amira$^{\mathrm{TM}}$.

To solve the system of partial differential equations of Problem 2.1 with the FE method (cf. Section 2.2), we used a code specially written to this end at our institute. This was done to gain performance by exploiting the special situation we were dealing with. The code has been tested by comparison with validated software.

For the numerical linear algebra, we chose the well validated software library SPOOLES [1], which is an optimized, multi-threaded package for the iterative solution of large, sparse linear systems by block LU decomposition. Together with heavy optimizations including parallelization

and use of hardware accelerated vector mathematics, this resulted in a runtime of 4.7 seconds per simulation (for a single load case) on a dual Intel Xeon processor with 1GB RAM. This allows the simulation to be used within the iterations of the algorithm for the solution of the inverse problem to be described in the following section, which involves a large number of evaluations per step.

2.4 Validation and determination of material parameters

Any numerical simulation has to be validated to confirm that it gives sensible predictions for the phenomena it is supposed to replicate. For that reason, a simulation was performed as described above, with the unknown material parameters replaced by guesses taken from the range reported in the literature. The results were then compared (only qualitatively, of course) with the experimental observations.

Based on this numerical simulation of the in vitro experiments, one can then formulate an approach to calculate the unknown material parameters from measurements. Mathematically, the simulation (and with it, the experiment it mirrors) takes the form of an operator equation $T(x) = u$, where T maps the vector of material parameters x (in our case, the E and ν for both the cortical and the cancellous bone) to the displacement field of the mandible under a given load. Here, we are interested in the *inverse problem*, namely the inverse operator T^{-1} which maps a given (i.e. measured) displacement field to the parameters involved.

Since the results of the simulation depend non-linearly on these parameters (in the form of the entries of the stiffness matrix), this problem is formally ill-posed, meaning for a given displacement, there may not exist a solution x, or if it does, it may not be unique (it might also not depend continuously on the data, cf. infra). In this case, we are looking instead for the Moore-Penrose inverse $T^\dagger$, which gives the least squares solution (of minimal norm) for $T(x) = u$ for any u in the domain of $T^\dagger$. In practice, this leads to output least squares: find $x^\dagger$ with

$$\left\|T(x^\dagger) - u\right\| = \inf\{\|T(z) - u\| \,|z \in \mathcal{D}(T)\}\,. \tag{8}$$

For the implementation, this infinite-dimensional problem has to be reduced to a finite dimensional setting. Rather than comparing the complete displacement field (which can not be measured in whole, as it is defined on the volume of the mandible), we restrict the comparison to six points chosen for good visibility from both cameras and covering an area of interest to the surgeons. In order to gather the necessary amount of data for the least-squares problem, we chose to compare the same experimental set-up under a reasonable number of different loads (in our case six). Hence, the discretized operator T_h corresponds to calculating, for given material parameters x, the displacement at these six points under the six different loads by FE simulation. Correspondingly, u_h becomes a vector of 108 measured components (6 points times 3 coordinates times 6 load cases). In this setting, the norms involved are then the Euclidean norms (square root of the sum of the squares of the components). The solution of this least squares problem should also properly be denoted by x_h, but we will drop this index for convenience.

However, due to the presence of measurement errors, we are dealing with u^δ, where

$$\left\|u^\delta - u\right\| \leq \delta\,,$$

and δ includes not only measurement errors, but also the error made by discretizing the inverse problem (which is not readily quantifiable). In this case $T^\dagger(u^\delta)$ is not a good approximation of $T^\dagger(u)$, since the problem is ill-posed: small differences in u can lead to arbitrarily large differences in $x^\dagger$. Stability can be restored by a pointwise approximation of the Moore-Penrose inverse, which adds a penalty term:

$$\left\|T(x) - u^\delta\right\|^2 + \alpha \|x\|^2 \to \min,\ x \in \mathcal{D}(T)\,. \tag{9}$$

This is called Tikhonov-regularization [7], which can be applied to the discretized problem in the same way. The correct choice of α is of critical importance; if the value is too large, the solution of (9) is far from the "real" x — too small, and convergence is lost. In the general case, several parameter choice rules exist, which can be shown to be optimal [26]. However, they assume knowledge of the noise level δ, which, due to the interplay of the various measurement and discretization errors, can not be characterized accurately enough here. Therefore, we use a different approach described further below.

Linearization by Taylor expansion around an estimate x_k^δ leads to the minimization of

$$\left\|u_h^\delta - T_h(x_k^\delta) - T_h'(x_k^\delta)(z - x_k^\delta)\right\|^2 + \alpha \left\|z - x_k^\delta\right\|^2 , \tag{10}$$

for $z = x_{k+1}^\delta$. Using Newton's method, the corresponding iteration scheme, starting from an estimate x_0^δ, is

$$x_{k+1}^\delta = x_k^\delta + ((T_h'(x_k^\delta))^T(T_h'(x_k^\delta)) + \alpha\mathbf{I})^{-1}(T_h'(x_k^\delta))^T(u_h^\delta - T_h(x_k^\delta)) . \tag{11}$$

Further stability can be gained by keeping the starting guess x_0 in the penalty term :

$$x_{k+1}^\delta = x_k^\delta + ((T_h'(x_k^\delta))^T(T_h'(x_k^\delta)) + \alpha\mathbf{I})^{-1}\left[(T_h'(x_k^\delta))^T(u_h^\delta - T_h(x_k^\delta)) + \alpha(x_0^\delta - x_k^\delta)\right] \tag{12}$$

This method was used in our study. For numerical reasons, it is better to rearrange the iteration rule and solve a system of linear equations for the update $x_{k+1}^\delta - x_k^\delta$. For clarity, we will also drop the superscript δ from here on.

Since the calculated displacements $T_h(x)$ depend in general only implicitly on the material parameters x, the Jacobian cannot be derived analytically. Hence, a finite difference approximation was used. In each iteration, the displacements corresponding to the current iterate x_k were evaluated. Then for each parameter in turn, a small perturbation ε was added and the new displacements calculated. The columns of the approximate Jacobian are thus (e_i denoting the i-th unit vector)

$$T_h'(x_k)_i = \frac{T_h(x_k + \varepsilon_i \cdot e_i) - T_h(x_k)}{\varepsilon_i} ,$$

resulting in a 108×4 matrix. According to the standard literature, the optimal tradeoff between the inevitable roundoff errors and discretization error is reached at $\varepsilon_i = \sqrt{\epsilon} \cdot x_{k,i}$, where ϵ denotes the machine accuracy (cf. [22, Section 5.7]).

In the absence of the necessary information on the noise level, we employ a strategy described in [27] to find the parameter α for which the solution of (12) is an approximation close to the optimum of (8).

Specifying an initial value α^0 and a starting guess x_0, we iterate (12) until the change in the residual

$$r_k = \left\|T_h(x_k) - u_h^\delta\right\|$$

drops below a given tolerance τ for the first time, say at step k with iterate $x^0 = x_k$. We then repeat the process with $\alpha^{s+1} = \mu\alpha^s$ and $x_0^{s+1} = x^s$ until a preassigned α^{s^*} is reached. The parameter $\alpha^s = \alpha^{\bar{s}}$ for which

$$\sigma(\alpha^s) = \left\|x^{s+1} - x^s\right\|$$

is minimal in value is taken as the optimal parameter and the corresponding $x^{\bar{s}} = x^*$ as the solution of the inverse problem.

Marker point	x coordinate	y coordinate	z coordinate
upper anterior	0.459	0.263	0.148
median anterior	0.165	0.090	0.150
lower anterior	0.164	0.074	0.145
upper posterior	0.165	0.130	0.117
median posterior	0.165	0.071	0.137
lower posterior	0.202	0.134	0.111

Table 1: Average relative mean square errors for the coordinates of the displacements of the tracked markers; dry mandible, load case 1:3.

Marker point	x coordinate	y coordinate	z coordinate
upper anterior	0.285	0.226	0.137
median anterior	0.132	0.073	0.138
lower anterior	0.144	0.080	0.140
upper posterior	0.126	0.081	0.120
median posterior	0.135	0.073	0.132
lower posterior	0.143	0.447	0.133

Table 2: Average relative mean square errors for the coordinates of the displacements of the tracked markers; dry mandible, load case 1:2.

For our problem, we chose $\alpha^0 = 1.0$, $\mu = \sqrt{0.1}$ and $\alpha^{s^*} = 10^{-9}$. The tolerance was set to $\tau = 1.1 \cdot 10^{-4}$. Starting values x_0^0 were taken from the range reported by the literature ($E_{\text{cortical}} =$ 10GPa, $E_{\text{cancellous}} = 1$GPa, $\nu_{\text{cortical}} = 0.30$, $\nu_{\text{cancellous}} = 0.30$). The data u_h^δ were set as the measured displacement vectors of the six points for loads ranging from 300N to 600N in steps of 50N. The full force was applied to the incisal area, while only one-third of this was applied to each of the muscle-sling areas. The material parameters were identified, and the corresponding displacements (for the full range of forces) were calculated and compared with the measurements. As a further validation, these same parameters were used to simulate load cases where the muscle areas were subjected to one half the force of the incisal bite and compared with the corresponding experimental data. The same procedure was then repeated with the soaked mandible.

3 Results

The first validation of the simulation with plausible material parameters showed a satisfactory qualitative agreement with the experimental observations (see Figure 4).

The parameter identification procedure for the dry mandible converged to the material parameters $E_{\text{cortical}} = 5.4666$GPa, $E_{\text{cancellous}} = 0.646425$GPa, $\nu_{\text{cortical}} = 0.246425$, $\nu_{\text{cancellous}} = 0.246425$. The displacements calculated with these parameters for the one-third load case, compared with the measured displacements at the six points under observation, are shown in the appendix (Figure 5). Here, the x-axis runs from dorsal to ventral, the y-axis from sinistral to dextral, and the z-axis from caudal to cranial. The average relative mean square errors (rounded to three decimal places) for the coordinates of the displacements of these points are given in Table 1.

The comparisons for the one-half load case are shown in Figure 6, the errors in Table 2.

The results of the parameter identification for the soaked mandible are $E_{\text{cortical}} = 5.65839$GPa, $E_{\text{cancellous}} = 0.785742$GPa, $\nu_{\text{cortical}} = 0.273068$, $\nu_{\text{cancellous}} = 0.269998$. The comparison of calculated and measured displacements for all loads with these parameters are shown in Figure 7 . The errors can be seen in Table 3.

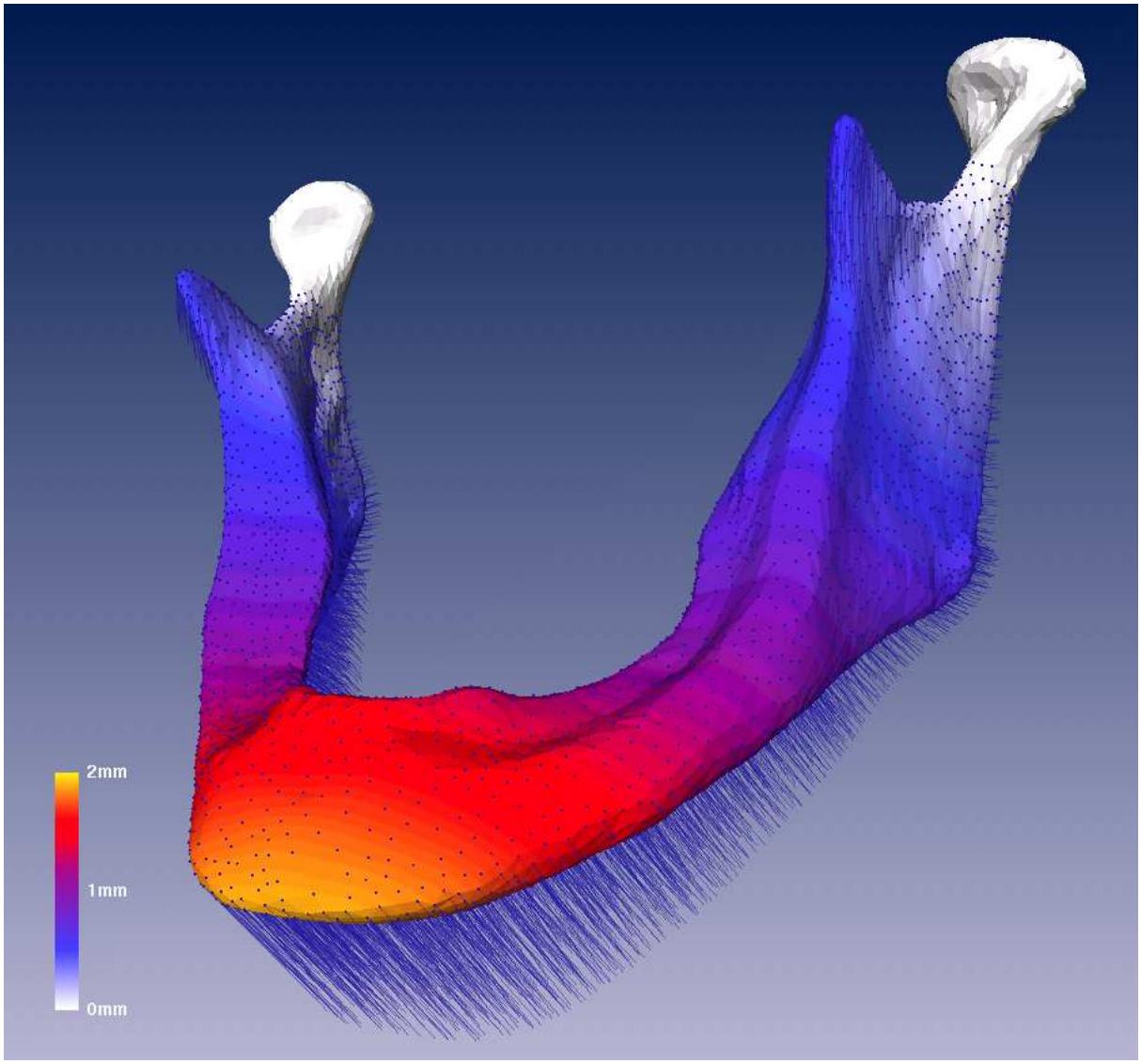

Figure 4: Results of simulation with estimated parameters. Vectors show displacements of the nodes, color coding shows the absolute magnitude of surface displacements.

Marker point	x coordinate	y coordinate	z coordinate
upper anterior	0.249	0.102	0.138
median anterior	0.142	0.249	0.138
lower anterior	0.143	0.101	0.143
upper posterior	0.165	0.130	0.117
median posterior	0.131	0.261	0.131
lower posterior	0.153	0.272	0.128

Table 3: Average relative mean square errors for the coordinates of the displacements of the tracked markers; soaked mandible, load case 1:3.

4 Discussion

The qualitative validation of the simulation showed good agreements with experimental observations. This allowed us to use the simulation for the parameter identification with confidence. The parameter identification routine yielded in both cases plausible values which were well within the range reported by the literature. With the calculated parameters, the quantitative agreement between measured and calculated displacements at the six points was good for all the load cases. Particularly the validation via the independent measurements for the one-half-load case, to which the parameters were *not* fitted, lends the results strength.

The least accurate match was observed (for all load configurations) at the upper anterior point, where we systematically underestimate Young's modulus. This could be explained by its location on top of the alveolar ridge, where the assumption of the material being cortical bone was most likely to be wrong, but the reason for the behavior of the upper anterior marker is currently unknown. In order to keep the specimen undamaged for further experiments, we refrained from histological examinations of the mandible. From the CT data alone, we were not able to exclude the existence of bony surrounded relics of a tooth, a former fracture, or an osteitis caused by permanent pressure effects from dental prostheses. All these effects could lead to a locally higher stiffness.

Of note is also the deviation of the medio-lateral (y) component of the displacements. This is likely to be the result of the relatively small value of the medio-lateral displacements compared to the manual tracking accuracy. Additionally, due to technical restrictions, only the camera with frontal view was able to quantify this direction fully. After tracking, the data were processed by SIMI°Motion^{TM}. Since the internal algorithms of this commercial motion capture software are not publically available, we can not be sure about the functional connection between the camera input and the computed medio-lateral movement in this case. But it seems that in the absence of fully independent measurements from two directions, small errors in the manual tracking can result in large variations in the calculated component of movement.

We have achieved our goal of creating a method for a parameter identification based on a numerical simulation which stays close to experiments, and which does not rely on external parameters for its accuracy. The pipeline described in Section 2.3 from a human mandible via CT scan to validation requires no external input. In consequence, the set-up is independent of the chosen specimen and can easily be extended to more complex models or load configurations; for example including further materials (e.g. teeth) or materials with anisotropy (by increasing the number of parameters to be identified). Indeed, the non-destructive nature of the approach would allow multiple tests on the same object for comparison.

This also is to our knowledge the first validation, qualitative as well as quantitative, of a numerical simulation of the elastic behavior of the mandible by experiments on the same object, under identical load configurations.

Among the future goals can be an application of our method to a series of specimen in order to make statistically significant estimates of average material properties of human mandibles. Moreover, this validated simulation (now with known parameters) can serve as a basis for the inclusion of more physiological conditions, by accounting for the TMJ. Under consideration is also an extension of the calculations to dynamical loads, for which the test bed is already equipped. Of interest for the clinical use is the inclusion of implants applied to the mandible. Finally, as a long term goal, it is planned to consolidate these components into an integrated tool for computer aided surgery planning.

Acknowledgements.

This work was supported by the Deutsche Forschungsgemeinschaft, project SFB 438, and the Klinikum rechts der Isar, TU München, grant KKF 45-98. The authors wish to thank Martin Brokate for continuing support, Jan Christoph Wehrstedt for our implementation of the finite

element method, Robert Sader and Hans-Florian Zeilhofer for valuable clinical input. Ludger Kirsch and Ulrich Thorns obtained the specimens. Rainer Burgkart, Andreas Kolk and Wolfgang Hauck helped by retrieving the required CT scans. In addition, Andreas Kuhn and Gabriele Mühlberger gave an essential introduction to mandibular surgery and related problems. Reiner Gradinger and Wolfram Mittelmeier host the Mandibulator at the Biomechanical lab, where Rainer Bader, Stefan Eichhorn, Ulrich Schreiber and Erwin Steinhauser gave steady technical support and advice.

Appendix.
Comparisons of measured and simulated displacements

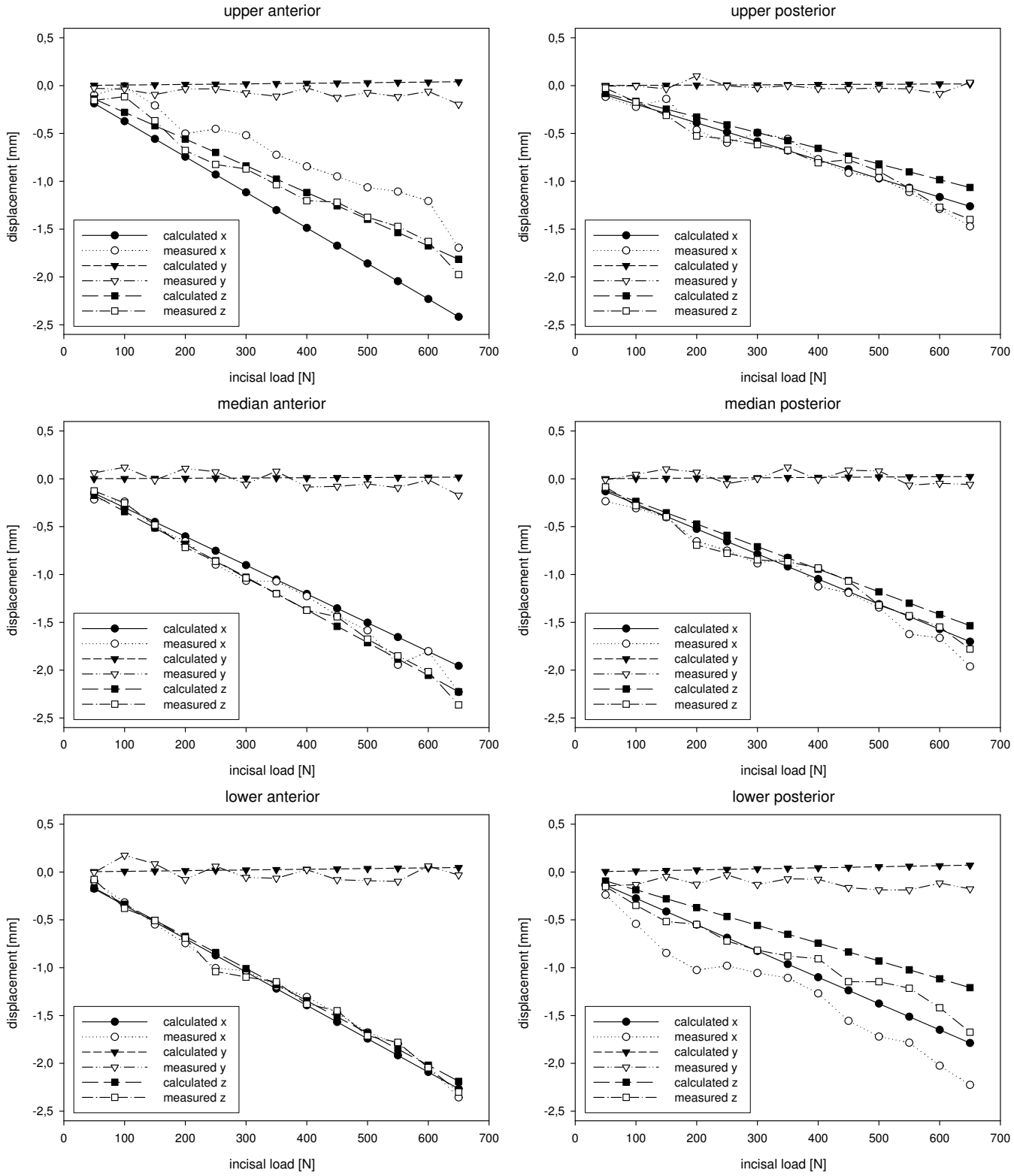

Figure 5: Comparison of measured and calculated components of displacement for the six marker points; dry mandible, loadcase 1:3

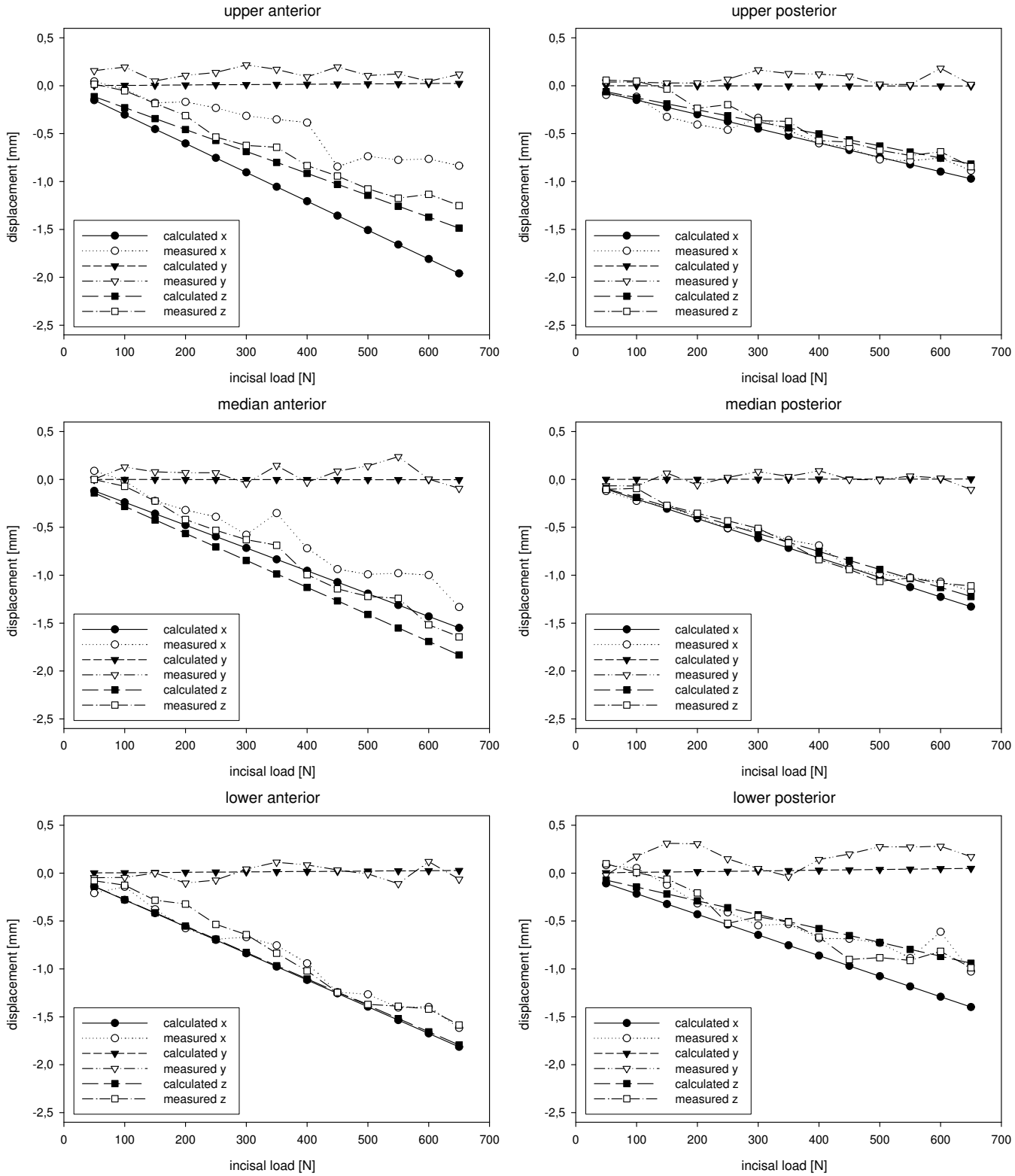

Figure 6: Comparison of measured and calculated components of displacement for the six marker points; dry mandible, loadcase 1:2

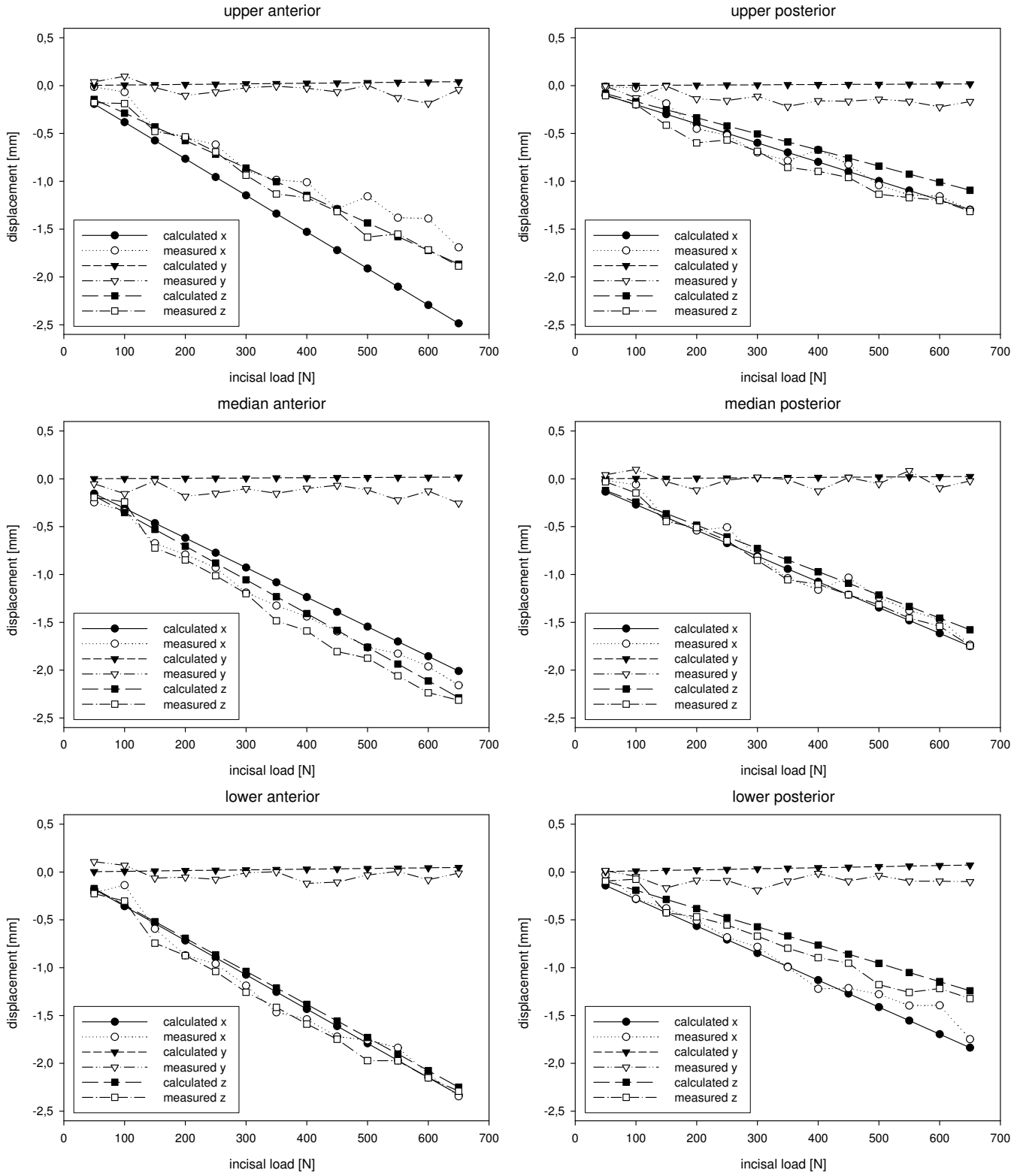

Figure 7: Comparison of measured and calculated components of displacement for the six marker points; soaked mandible, loadcase 1:3

References

[1] C. Ashcraft, R. Grimes (1999), SPOOLES: An object-oriented sparse matrix library. *Proceedings of the 9th SIAM Conference on Parallel Processing for Scientific Computing*, San Antonio, CD-ROM.

[2] M. Beek, J.-H. Koolstra, J. van Ruijven, T. M. G. J. van Eijden (2000), Three-dimensional finite element analysis of the human temporomandibular joint disc. *Journal of Biomechanics* **33**, 307–316.

[3] D. Braess, *Finite Elements: Theory, Fast Solvers, and Applications in Solid Mechanics* (Cambridge University Press, Cambridge, 2001).

[4] P. G. Ciarlet, *The Finite Element Method for Elliptic Problems* (North-Holland, Amsterdam, 1978).

[5] P. G. Ciarlet, *Mathematical Elasticity, Volume I: Three-Dimensional Elasticity* (North-Holland, Amsterdam, 1988).

[6] L. Cristofolini, M. Viceconti (2000), Mechanical validation of whole bone composite tibia models. *Journal of Biomechanics* **33**, 279–288.

[7] H. W. Engl, M. Hanke, A. Neubauer, *Regularisation of Inverse Problems* (Kluwer Academic Publishers, Dordrecht, 1996).

[8] J. R. Fernández, M. Gallas, M. Burguera, J. M. Viaño (2003), A three-dimensional numerical simulation of mandible fracture reduction with screwed miniplates. *Journal of Biomechanics* **36**, 329–337.

[9] T. Gay, J. Rendell, A. Majoureau, F. T. Maloney (1994), Estimating human incisal bite forces from the electromyogram bite-force function. *Archives of Oral Biology* **39**, 111–115.

[10] R. T. Hart, V. V. Hennebel, N. Thongbreda, W. C. van Buskirk, R. C. Anderson (1992), Modeling the biomechanics of the mandible: A three-dimensional finite element study. *Journal of Biomechanics* **25**, 261–286.

[11] J. Kabel, B. van Rietbergen, M. Dalstra, A. Odgaard, R. Huiskes (1999), The role of an effective isotropic tissue modulus in the elastic properties of cancellous bone. *Journal of Biomechanics 32*, 673–680.

[12] T. Kampe, T. Haraldson, H. Hannerz, G. E. Carlsson (1987), Occlusal perception and bite force in young subjects with and without dental fillings. *Acta Odontologica Skandinavica* **45**, 101–107.

[13] P. Knabner, L. Angermann, *Numerical Methods for Elliptic and Parabolic Partial Differential Equations* (Springer, Berlin, 2003).

[14] J. H. Koolstra, T. M. G. J. van Eijden (1999), Three-Dimensional Dynamical Capabilities of the Human Masticatory Muscles. *Journal of Biomechanics* **32**, 145–152.

[15] J. H. Koolstra, T. M. G. J. van Eijden (2001), A method to predict muscle control in the kinematically and mechanically indeterminate human masticatory system. *Journal of Biomechanics* **34**, 1179–1188.

[16] J. H. Koolstra, T. M. G. J. van Eijden, W. A. Weijs, M. Naeije (1988), A three-dimensional mathematical model of the human masticatory system predicting maximum possible bite forces. *Journal of Biomechanics* **21**, 563–576.

[17] T. W. P. Korioth, D. P. Romilly, A. G. Hannam (1992), Three-Dimensional Finite Element Stress Analysis of the Dentate Human Mandible. *American Journal of Physical Anthropology* **88**, 69–96.

[18] B. May, S. Saha, M. Saltzman (2001), A three-dimensional mathematical model of temporomandibular joint loading. *Clinical Biomechanics* **16**, 489–495.

[19] C. Meyer, J.-L. Kahn, P. Boutemy, A. Wilk (1998), Determination of the external forces applied to the mandible during various chewing exercises. *Journal of Cranio-Maxillofacial Surgery* **26**, 331–341.

[20] A. N. Natali, E. A. Meroi, (1988), A review of the biomechanic properties of bone as a material. *Journal of Biomechanical Engineering* **11**, 266–275.

[21] A. Neff, A. Kuhn, H. Schieferstein, A. M. Hinz, E. Wilczok, G. Mühlberger, H.-F. Zeilhofer, R. Sader, H. Deppe, H.-H. Horch (2000), Development of Innovative Osteosynthesis Techniques by Numerical and In Vitro Simulation of the Masticatory System. In *Lectures on Applied Mathematics* (ed. H.-J. Bungartz, R. H. W. Hoppe, C. Zenger), Springer, Berlin, pp. 179–205.

[22] W. H. Press, S. A. Teukolsky, W. T. Vetterling, B. P. Flannery, *Numerical recipes in C* , 2nd ed. (Cambridge University Press, Cambridge, 1992).

[23] J. W. Osborn, F. A. Baragar (1985), Predicted pattern of human muscle activity during clenching derived from a computer assisted model: Symmetric vertical bite forces. *Journal of Biomechanics* **18**, 599–612.

[24] J.-Y. Rho, R. B. Ashman, C. H. Turner (1993), Young's modulus of trabecular and cortical bone material: ultrasonic and microtensile specimens. *Journal of Biomechanics* **26**, 111–119.

[25] H. Schieferstein, *Experimentelle Analyse des menschlichen Kausystems* (Herbert Utz Verlag, München, 2003).

[26] U. Tautenhahn (1997), On a general scheme for nonlinear ill-posed problems. *Inverse Problems* **13**, 1427–1437.

[27] A. N. Tikhonov, V. B. Glasko (1965), Use of the regularization method in non-linear problems. *USSR Computational Mathematics and Mathematical Physics* **5**, 93–107.

[28] V. Vitins, M. Dobelis, J. Middleton, G. Limbert, I. Knets (2003), Flexural and Creep Properties of Human Jaw Compact Bone for FEA Studies, *Comput. Methods Biomech. Biomed. Engin.* **6**, 299–303.

[29] H.-F. Zeilhofer, *Innovative dreidimensionale Techniken — Medizinische Rapid Prototyping-Modelle für die Operationsplanung und daraus resultierende neue Entwicklungen in der Mund-Kiefer-Gesichtschirurgie* (Thesis of Habilitation, TU München, 1998).